# Density-functional calculation of the shock Hugoniot for diamond

Nichols A. Romero and William D. Mattson
*U.S. Army Research Laboratory, Aberdeen Proving Ground, Maryland 21005-5066, USA*
(Received 13 March 2007; published 20 December 2007)

The principal Hugoniot of diamond is calculated using density-functional molecular dynamics. Using existing *ab initio* melt lines, diamond is predicted to melt on its Hugoniot in the range of 700–745 GPa. The shock compression of diamond into a high-density conducting liquid phase has an associated 13%–14% density increase across its coexistence region. Complete band gap closure before the onset of melting is not observed within these calculations. The importance of two simulation parameters necessary for obtaining quantitatively accurate predictions in the liquid carbon phase is identified: electronic temperature and supercell size. Our results expound upon existing laser-driven shock experiments and provide valuable equation of state data relevant to future high-pressure physics experiments.

DOI: 10.1103/PhysRevB.76.214113 PACS number(s): 62.50.+p, 64.30.+t, 71.15.Mb, 61.20.−p

## I. INTRODUCTION

The properties of carbon at extreme conditions are of particular interest to the astrophysical sciences[1] and shock wave physics.[2] Carbon's most well-known allotropes are graphite and diamond, the latter being its ground state at room temperature and pressures as low as 1 GPa.[3] Diamond is the hardest naturally occurring material; used in diamond anvil cells (DACs) to achieve hydrostatic pressures of several hundred GPa. As a result of its incompressibility and extreme stability,[4] it has proven difficult to study the carbon equation of state (EOS) at the high pressures and temperatures needed to melt diamond. The experiment of Shaner *et al.*[5] demonstrated that shock compressed graphite would remain in its diamond phase up to 140 GPa and 5600 K. Diamond has also been shock compressed up to 585 GPa by Pavlsokii[6] without the observation of a solid-liquid phase transition. Two laser-generated shock wave experiments[7,8] have probed the carbon EOS in the terapascal regime, but are not in agreement on the state of carbon at these ultrahigh pressures and temperatures. The difficulty in studying carbon at these extreme conditions has motivated a large number of *ab initio* simulations.

The first-principles density-functional theory (DFT)[9] method has repeatedly demonstrated itself as a powerful tool to predict the properties of matter at extreme conditions[10,11] as well as to assist in the interpretation of shock experiments.[12,13] There is a long history of its application to carbon at extreme conditions. In 1990, Galli *et al.* applied the method to liquid carbon,[14,15] and the melting of diamond.[16] A few years later, the work of Grumbach and Martin[17] predicted a phase diagram for carbon which included a reentrant melt line and two high density phases (BC-8 and simple cubic) existing above 1 TPa. More recently, Wang, Scandolo, and Car (WSC)[18] provided a more accurate calculation of the diamond melt line; with their results demonstrating some of the shortcomings of empirical methods. Lastly, Correa, Bonev, and Galli (CBG)[19] published an *ab initio* phase diagram of carbon which included diamond and BC-8 melt lines, BC-8/diamond phase boundary, and a partial shock Hugoniot in the diamond phase up to its melt line.

Experiments performed by a team of scientists from Lawrence Livermore National Laboratory (LLNL) reported the melting of diamond to a conducting liquid between 600 and 1000 GPa along its principal Hugoniot.[7] In contrast, the experiments of a multi-institute collaboration in Japan did not make the assertion of a phase transition,[8] but were able to provide valuable Hugoniot data with definitive error bars. We calculate the principal Hugoniot of diamond using DFT and use the existing melt lines of WSC and CBG to make predictions. Our calculations augment the existing CBG data and provide valuable shock Hugoniot results in the liquid phase for pressures up to 1.4 TPa. The comparison with the existing laser-driven shock experiments serves to validate the accuracy of DFT for this application as well as providing information valuable to the interpretation of present and future laser shock experiments. We also compare our results to the EOS model of Fried and Howard (FH).[20] This latter comparison is useful for assessing the strengths and weaknesses of similar EOS constructions and may provide insights on how to improve existing models.

## II. COMPUTATIONAL METHOD

The principal Hugoniot requires accurate calculation of the internal energy and pressure of a system at a given density and temperature. We choose to compute these thermodynamic quantities using Kohn-Sham (KS)[21] DFT as implemented in the Vienna *ab initio* simulation program (VASP)[22] code developed at the Technical University of Vienna. Our thermodynamic quantities are computed by performing Born-Oppenheimer molecular dynamics (MD) in the canonical ensemble using a Nosé-Hoover thermostat for the ions.[23] The core electrons are replaced with hard projector-augmented-wave (PAW) potentials from the VASP library.[24] The exchange-correlation energy uses the generalized gradient approximation (GGA) of Perdew-Berke-Ernzerhof.[25] The following paragraphs discuss several distinct sources of systematic errors in our calculation. Before proceeding further, it is worth noting that two of these sources could not be assessed. The first arises from the approximation to the exchange-correlation energy; although there are more accurate functionals, e.g., exact exchange,[26] and more accurate quantum mechanical methods, e.g., quantum Monte Carlo, they are currently computationally intractable for performing MD. Secondly, the PAW approximation could not be tested with more accurate potentials constructed using smaller radii

 

since there is no facility for generating them within the VASP software package. However, it should be noted that the work of Kunc *et al.*[27] demonstrated that the hard PAW potentials from the VASP library are consistent with the zero-temperature EOS of diamond up to 600 GPa as obtained by the more accurate augmented plane-wave + local orbital method.

These DFT calculations have two major sources of convergence errors: the energy cutoff controlling the basis set size and the finite-size effect. The VASP code expands the electronic states using a plane-wave basis. The accuracy of the electronic states is controlled by the plane-wave energy cutoff $E_c$. The results presented here use $E_c=875$ eV and a 64-atom simple-cubic supercell. It is well known that the pressure is slower to converge with respect to $E_c$ than the KS energy.[28] Calculations on the solid diamond phase determined that increasing $E_c$ to 950 eV changed the KS energy and pressure by $<1$ meV/atom and 0.7 GPa, respectively. Similar changes were found in the liquid phase. Our choice of $E_c$ results in a negligible error in the KS energy, and no more than a 1% error for pressures in the strong shock regime. The nonlocal projectors for the PAW potentials are evaluated in real space and optimized by the method of Kresse.[29] While the nonlocal projectors are known to be more accurately evaluated in reciprocal space, the real-space projectors are faster to evaluate and exhibit better scaling with system size. In order to appropriately balance accuracy and performance, the real-space projectors were optimized with a strict tolerance in order to minimize systematic errors in the energies and pressures.

In periodic systems, $k$-point sampling is routinely employed to reduce the electronic finite-size effect. As the systems considered here are a warm dense solid diamond and a liquid carbon phase, the $k$-point sampling does not reduce the electronic finite-size effects in exactly the same manner as it would for a perfectly ordered crystalline solid. It is, in fact, more appropriate to assess the electronic finite-size effects by using larger supercells rather than increased $k$-point sampling. However, it is worth noting that there are demonstrations in the literature[30] of electronic finite-size effects for disordered systems which are captured by increased $k$-point sampling. In our calculations, only the $\Gamma$ point is sampled to minimize the computational cost of our DFT-MD. Calculations performed at $E_c=875$ eV on 64-, 128-, and 256-atom supercells for the lowest and highest densities studied in the diamond phase determined that KS energy is converged to about 80–140 meV/atom while the pressure is converged 1.3–3.8 GPa; with a larger convergence error at higher densities due to the increased size of the Brillouin zone (BZ). This finite-size effect contributes an additional error of 1%–2% and 1% in the KS energy and pressure, respectively. Since the total internal energy $E$ is the sum of the KS energy $E_{\mathrm{KS}}$ and the kinetic energy of the ions, an error in the KS energy $\delta E_{\mathrm{KS}}$ could be expected to give an error in the Hugoniot temperature on the order of $\delta E_{\mathrm{KS}}/(3/2k_{\mathrm{B}})$. However, the finite-size effect error in the Hugoniot temperature is reduced through a cancellation of error since the energies of the final (shocked) state are taken with respect to an initial (unshocked) state which also exhibits a finite-size effect with the same sign, albeit smaller in magnitude. Lastly, the finite-size effect error in the pressure, which enters into the Hugoniot relation as product of the form $(P+P_0)(\rho-\rho_0)$, further reduces the error in the Hugoniot temperature. We estimate our finite-size error in the Hugoniot temperatures to be no more than $\sim$60 K for the highest densities considered in the solid diamond phase.

A similar finite-size convergence test on the liquid carbon phase showed changes of 110–120 meV/atom and 10 GPa in the KS energy and pressure, respectively. These larger errors are due to $\Gamma$-point sampling of the liquid carbon phase which is known to be metallic.[14–17] The calculated pressure is still about 1% of typical pressures found in the high-density liquid carbon regime. These finite-size errors in the KS energy and pressure lead to errors in the Hugoniot temperatures of about 200–300 K for the density ranges considered for the liquid carbon phase. It would be of significant interest to determine if the finite-size error in the liquid phase increases substantially at higher densities as was observed in the diamond phase. This would be necessary for accurate predictions at the densities relevant for inertial confinement fusion. Nevertheless, we regard our calculations in the liquid carbon phase as the next step toward a more quantitative Hugoniot prediction for this system.

The last parameter in our DFT calculation that we consider is the electronic temperature $T_e$. Although $T_e$ is typically regarded as a convergence parameter for reducing the computational cost associated with gapless systems, recent works[11,31] have demonstrated that a finite-temperature treatment of the electronic degrees of freedom gives a thermal ground state which is physically meaningful and substantially different from those neglecting thermally occupied states ($T_e=0$). The first-principles shock Hugoniot of Militzer *et al.*[11] for liquid helium demonstrated that DFT-MD results corrected for thermal electronic excitations yield better agreement with path integral Monte Carlo calculations. In a notable DFT study on high energy-density water,[31] the incorporation of thermally excited electrons was shown to dramatically change the electronic structure. The electronic states in our DFT-MD were occupied using a Fermi-Dirac distribution. Several tests demonstrated no significant differences between $T_e=0$ K and $T_e=T$ in the solid diamond phase except near the CBG and WSC melt lines where a finite occupation of thermally excited states was found to slightly increase the Hugoniot temperature. In sharp contrast, thermally excited states lead to non-negligible changes in our interpolated Hugoniot values for the liquid carbon phase, but did not otherwise affect its fundamental character in an analogous manner to that observed in the case of high energy-density water. In this paper, we denote $T_e=T$ results by the abbreviation fTe.

## III. RESULTS AND DISCUSSION

The thermodynamic states accessible under shock conditions are given by the Hugoniot which is the locus of points in $(E,P,\rho)$ space satisfying the condition[32]

$$h(\rho,T)=E-E_0+\frac{1}{2}\left(\frac{1}{\rho}-\frac{1}{\rho_0}\right)(P+P_0)=0, \qquad (1)$$

where $E$ is the internal energy per unit mass, $P$ is the pressure, $\rho$ is the density, and the subscript 0 denotes the initial

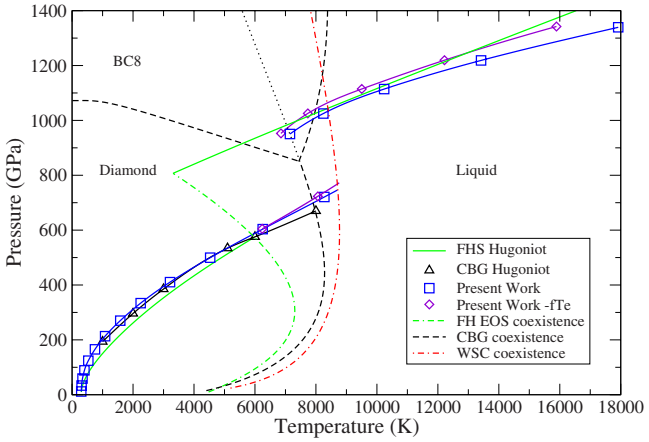


FIG. 1. (Color online) Diamond Hugoniot from present work (blue squares; purple diamonds denote fTe) superimposed on the *ab initio* phase diagram of CBG (Ref. 19; dashed black) including the metastable extension of the diamond melt line (dotted black) along with the diamond melt line of WSC (Ref. 18; dash-dotted red), and the FH EOS (Ref. 20; double-dash dotted green). The shock Hugoniot of FH EOS (solid green) and CBG (black triangles) are included for comparison. The diamond melt line data of WSC are fitted to the Kechin model (Ref. 39).

state. The Hugoniot function $h(\rho,T)$ is calculated by the Erpenbeck[33] equation of state method. The Hugoniot state variables are interpolated at each density by computing $h(\rho,T)$ at a number of different temperatures. For the *principal* Hugoniot, the initial state was taken to be unshocked diamond with $\rho_0=3.473$ g/cm$^3$, $T=300$ K, and $P_0\approx 0$ GPa, which is close to its experimental density of 3.51 g/cm$^3$ at ambient conditions. Our calculations were all performed on a 64-atom simple-cubic supercell isotropically strained to obtain the desired density. We took the pressure in the Hugoniot equation to be the hydrostatic pressure on this supercell. This hydrostatic Hugoniot (hydrostat) is different from the experimental Hugoniot, but should only differ by two-thirds the yield strength (on the order of 20 GPa)[34] above the Hugoniot elastic limit which may be as high as 110 GPa.[34] Each Hugoniot point is first equilibrated over a long trajectory before taking thermodynamic averages for a period no less than 6 ps using 1 and 0.5 fs time steps in the solid and liquid phases, respectively.[35] Our MD simulation times are sufficiently long so that the statistical errors are significantly smaller than the convergence errors discussed in the previous sections. The largest sources of error for the temperature and pressure are the finite-size errors. The interpolated Hugoniot and EOS data are provided in the Appendix.[36]

Our principal Hugoniot is presented in Fig. 1 along with the *ab initio* results of WSC[18] and CBG,[19] plus the FH[20] EOS results. In a simple melting transition, there are discontinuities in the slope of the Hugoniot at two distinctive pressure-temperature points, $(P_s,T_s)$ and $(P_l,T_l)$, where the Hugoniot enters and exits the coexistence region. Below $(P_s,T_s)$ and above $(P_l,T_l)$, the material behind the shock wave is entirely solid and liquid, respectively. While between $(P_s,T_s)$ and $(P_l,T_l)$, the Hugoniot follows the melt line and Eq. (1) can be solved by assuming that the extensive thermodynamic variables interpolate linearly according to their mixed-phase volume fraction $[V=(1-\lambda)V_s+\lambda V_l]$. As an independent calculation of the diamond melt line was not performed, the principal Hugoniot is not given in the coexistence region. Instead the principle Hugoniot from this work consists of two disconnected solid and liquid branches.

One of the most striking features of Fig. 1 is that there are significant differences at high pressures between the calculated diamond melt lines including those obtained with DFT. The large disagreement with the FH EOS is not unexpected as it was paramterized using the older *ab initio* data of Grumbach and Martin[17] (not depicted in Fig. 1). The two more recent melt lines of WSC and CBG are in better agreement with one another, yet have a fair amount of disagreement at higher pressures which is larger than typical sources of convergence errors. This is undoubtedly related to the delicate computational nature of determining phase boundaries. Although the cause (e.g., pseudopotentional, MD method, or coexistence approach[37]) of these differences is worth further exploration, we take these DFT melt lines as given and make predictions based on them rather than independently calculating a diamond melt line. In the work of CBG, BC8-liquid coexistence was also considered. Our predictions assume the Hugoniot follows the metastable diamond melt lines of CBG or WCS; BC8-liquid coexistence was not considered. Our DFT-MD calculations were performed only on the diamond and liquid phases. While it follows from the CBG phase diagram that the Hugoniot traverses the BC8-liquid melt line before exiting into the pure liquid phase region, *ab initio* calculations have determined that diamond under fast compression survives in a metastable state up to about 3 TPa.[38] None of our calculations are able to elucidate this point.

Our present work predicts that diamond would melt either at 700 GPa, 7900 K or 745 GPa, 8700 K on the principal Hugoniot using the CBG and WCS melt lines, respectively. These pressures are within the broad range (600–1000 GPa) reported by the LLNL laser shock experiment.[7] Our calculated Hugoniot is in good agreement with that of CBG which used a 64-atom supercell and $T_e=0$ K. The main distinction between our calculations is that their EOS points were obtained using the norm-conserving pseudopotential method with thermodynamic averaging in the *NPT* ensemble. In sharp contrast, the FH EOS predicts melting to occur at a much lower pressure along the Hugoniot of 574 GPa with an associated temperature of 5980 K. The corresponding location where the Hugoniot exits the diamond-liquid coexistence region is predicted to be about 975 GPa, 7070 K and 1065 GPa, 8370 K for the CBG and WCS melt lines, respectively, while the FH EOS result is significantly lower in pressure and temperature. Figure 1 shows that although the FH EOS predicts a very different melt line, the predicted principal Hugoniot (solid green) closely tracks our present work in the diamond and liquid phases. This is suggestive that improvements to existing EOS models may be achieved by simply updating existing fitting parameters to reflect more recent *ab initio* results. Whether this is indeed the case is also worth further investigation but outside the scope of this study.

The results depicted in Fig. 1 also quantify the role of thermally excited electrons. Our shock Hugoniot was calcu-

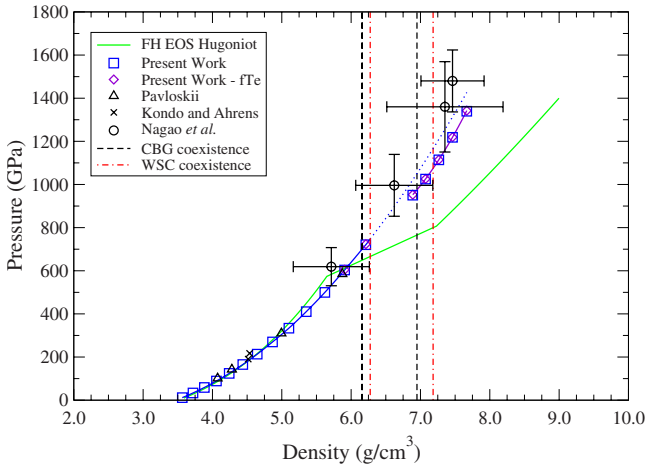


FIG. 2. (Color online) Calculated Hugoniot of diamond (blue squares; purple diamonds denote fTe) is plotted in the pressure-density plane along side the FH EOS (Ref. 20; solid green). The pressure-density data correspond to the pressure-temperature range depicted in Fig. 1. The experimental data of Pavloskii (Ref. 6; black triangles), Kondo and Ahrens (Ref. 34; black crosses), and Nagao *et al.* (Ref. 8; black circles) reflected-light measurements are also shown. The vertical lines correspond to the coexistence density range for the CBG (Ref. 19; dashed black) and WSC (Ref. 18; dash-dotted red) melt lines. The Hugoniot data in the solid diamond phase are extrapolated to densities considered in the liquid carbon phase (dotted blue).

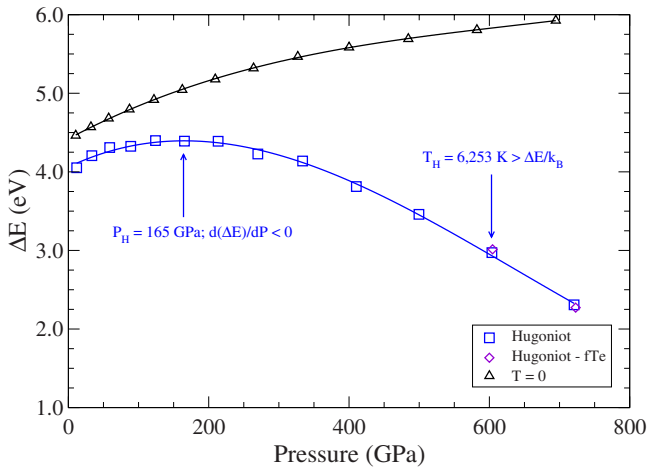


FIG. 3. (Color online) The energy gap $\Delta E$ for the highest and lowest occupied states at the $\Gamma$ point between zero-temperature crystalline diamond ($T=0$ K; black triangles) and along the principal Hugoniot (blue squares; purple diamonds denote fTe). The solid lines are a linear least squares fit to a cubic polynomial.

lated with $T_e=0$ K and $T_e=T$ (fTe) for all the Hugoniot points in the liquid and the two Hugoniot points in the solid which are closest to the *ab initio* melt lines. Similar to the calculation of CBG, we find that $T_e$ has little to no effect in the solid diamond phase except near the melt line (see Table I). In the liquid carbon phase, thermally excited electrons do not appear to fundamentally change the electronic structure. However, a comparison of the EOS points in Table II shows that while the pressure remains relatively unaffected by $T_e$, there are non-negligible increases in the internal energy. While these increases are not substantial for liquid carbon near the melt line, significant changes are found at higher densities which result in a large reduction of the Hugoniot temperatures.

The principal Hugoniot from this present work is also plotted in the pressure-density plane in Fig. 2. It is in excellent agreement with the earlier experiments of Pavloskii,[6] Kondo and Ahrens,[34] and within the error bars of the Nagao *et al.*[8] reflected-light measurements.[40] We have also extrapolated the solid diamond branch of the Hugoniot to densities studied in the liquid carbon phase. Figure 2 shows that the high-density extrapolation of the solid diamond Hugoniot (dotted blue) does not differ substantially from the results obtained in the liquid branch of the Hugoniot. Therefore, as asserted by Nagao *et al.*,[8] the density change associated with the melting of diamond is too small to detect within their experimental error. Our calculations predict a fractional density $(\rho_l-\rho_s)/\rho_s$ increase of 13%–14% across the coexistence region using the WSC and CBG data, while the FH EOS overpredicts this increase. The density increase described here pertains to the ingress and egress of the Hugoniot in the coexistence region. This density increase arises from melting at constant-$P,T$ (from the Clausius-Clapeyron equation) plus a cooling and pressure increase effect along the Hugoniot. We believe that additional Hugoniot measurements, particularly in the coexistence region, and further density-functional calculations are necessary to distinguish the melting of diamond from ultrahigh-pressure diamond.

The issue of band gap closure before the onset of melt is of particular interest to shock wave physics. Our $\Gamma$-point DFT-MD simulations do not allow us to study the indirect band gap $(\Gamma\rightarrow 0.74X)$[41] of diamond along its principal Hugoniot. The energy gap $\Delta E$ (defined when $T_e=0$) for our 64-atom supercell corresponds to the gap at $\Gamma\rightarrow 0.5X$ in the folded BZ of the primitive two-atom unit cell. Figure 3 compares the $\Delta E$ of diamond at zero temperature ($T=0$ K) and along the principal Hugoniot. For zero-temperature diamond, $\Delta E$ was found to be 0.32 and 0.47 eV larger than the indirect gap at the lowest and highest densities considered in this work, respectively. However, since it is known that the pressure coefficients for transitions to other conduction states along $\Gamma$ to $X$ are similar,[42] the expected difference between $\Delta E$ and the indirect gap along the Hugoniot should be about the same. As previously stated, our calculations were performed under hydrostatic pressure conditions. It is worth noting that the effects of anisotropic stress on the band gap of diamond have been previously reported in the literature[43] and are quantitatively different from those obtained under isotropic compression. Although this is clearly relevant to the large anisotropic stresses which can be found in DAC experiments, its relevance to the interpretation of shock data is not clear.

It is well known that carbon diamond's positive pressure derivative near the $X$ point is unique among diamond- and zinc-blende structures.[42] Figure 3 shows that isotropic compression is insufficient for complete band gap closure along the Hugoniot. The band gap reduction does not arise from an

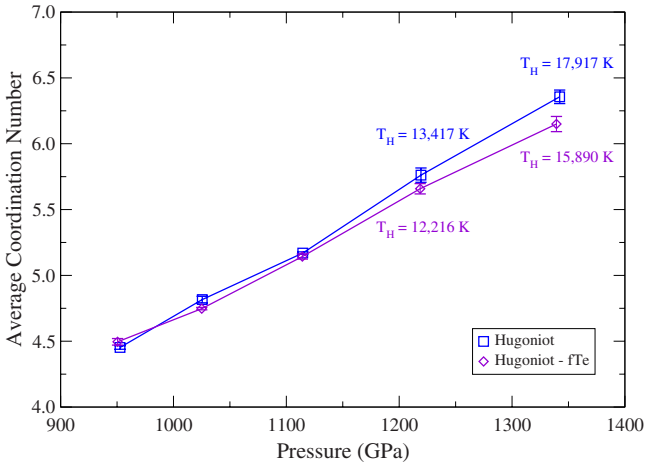


FIG. 4. (Color online) Average coordination number for the liquid branch of the principal Hugoniot (blue squares; purple diamonds denotes fTe). Interpolation errors for the average coordination number are included. The solid lines are only a guide for the visualization of trends.

increase in pressure but from thermal ionic motion and is evident even for the lowest Hugoniot temperature ($T_H$) at 300 K. Our calculations show that $\Delta E$ does not begin to decrease along the Hugoniot until approximately 165 GPa and never decreases below 2.0 eV before melting. It is only for temperatures exceeding the penultimate Hugoniot point ($T_H$=6253 K) that $\Delta E$ is sufficiently reduced to achieve thermal occupation of excited states. Our comparison of $T_e$ =0 K and $T_e$=$T$ demonstrates that the interpolation of relevant quantities is not significantly affected except for the value of $T_H$ which decreased by about 200 K for our last Hugoniot point (see Table III). Hence, the EOS points in the solid phase and interpolated Hugoniot data are more sensitive to the value of $T_e$ near WSC and CBG melt lines due to the reduction in the band gap.

Lastly, our long MD trajectory permitted the accurate computation of radial distribution functions. The average coordination number was computed by summing the radial distribution function up to its first minimum. Our calculations determined that the coordination number in the solid phase remained at four all the way up to the WSC and CBG melt lines, indicating that carbon did not undergo any structural transformation, remaining in its diamond phase even at the extreme temperatures and pressures. Therefore, Fig. 4 only plots the average coordination number for the liquid branch of the principal Hugoniot. All the coordination numbers in the liquid exceeded four, indicating that the Hugoniot intersects the melt line in the higher-density liquid phase which Grumbach and Martin associated with a positive melting slope $dT_m/dP$. Our average coordination numbers ranged from 4.5 to 6.5 which are lower than the range predicted by Grumbach and Martin, 6–7, but are more in line with those reported by CBG. The differences in the coordination number between $T_e$=0 K and $T_e$=$T$ arise primarily from changes in $T_H$. Hence, the observed increases in coordination number are correlated with an increase in the Hugoniot temperature and not to characteristic changes in the liquid (see Table IV). We have annotated $T_H$ to our last two data points in Fig. 4 to illustrate this point.

## IV. CONCLUSIONS

Density-functional calculations indicate that shock compressed diamond will melt into its high-density conducting liquid phase between 700 and 745 GPa on its principal Hugoniot. This is within the broad range reported by the LLNL experiment.[7] The results reported here are also within the error bars of the laser shock experiments of Nagao *et al.*[8] Our calculations indicate that the density increase for diamond due to melting along the Hugoniot is 13%–14% and would be difficult to distinguish experimentally from ultrahigh-pressure diamond without additional Hugoniot data in the coexistence region. We have pointed out that existing DFT melt lines[18,19] for diamond appearing in the literature disagree at high pressures beyond that which is expected from convergence errors. This clearly demonstrates the need to investigate sources of systematic error in future density-functional calculations of high-pressure melt lines. Two additional simulation parameters that are important for quantitative Hugoniot predictions in the liquid carbon phase are identified: electronic temperature and supercell size. A comparison between the results presented here and the FH[20] EOS shows that the principal Hugoniot is closely tracked in the diamond and liquid phases even though the FH EOS and *ab initio* melt lines of WSC[18] and CBG[19] are significantly different. The principal Hugoniot in the solid diamond phase appears to be in good agreement with the FH EOS model and the results of CBG. Our calculations find a reduction in the band gap along the Hugoniot, but closure before the onset of melt is not observed within GGA to DFT. This final point depends heavily on the elastic properties of diamond under shock conditions which was not considered in this work.

## ACKNOWLEDGMENTS

The authors would like to thank J. K. Brennan, K. P. Esler, and B. M. Rice for numerous useful discussions. In particular, we thank A. Kotlar for independently testing our least squares fit and error propagation codes. A. Correa provided the raw data published in Ref. 19. J. Eggert assisted in reproducing the results from Ref. 20 and provided many insightful comments. These calculations were performed on the Compaq SC45, HP XC, and SGI Altix 3700 at the Aeronautical Systems Center Majored Shared Resource Center. N.A.R. acknowledges support from the Research Associateship Programs of the National Research Council.

## APPENDIX: EOS AND HUGONIOT DATA

Tables I and II present our EOS data in the carbon diamond and liquid phase, respectively. This EOS data was used to interpolate the solid and liquid branch of the Hugoniot which are presented in Tables III and IV, respectively.

TABLE I. Equation of state data used in interpolating the Hugoniot data presented in Table III. Quantities enclosed in square brackets were obtained with $T_e=T$ while unbracketed quantities were obtained with $T_e=0$ K. The reference state is $\rho_0=3.473$ g/cm$^3$, $T_0=300$ K, $P_0\approx 0$ GPa, and $E_0=-8.89$ eV/atom

| $\rho$ (g/cm$^3$) | $T$ (K) | $P$ (GPa) | $E$ (eV/atom) |
|---|---|---|---|
| 3.564 | 200 | 11.4 | −8.914 |
| | 250 | 11.6 | −8.901 |
| | 300 | 11.9 | −8.888 |
| | 350 | 12.0 | −8.876 |
| 3.719 | 75 | 32.5 | −8.915 |
| | 200 | 32.9 | −8.883 |
| | 300 | 33.3 | −8.858 |
| | 400 | 33.9 | −8.831 |
| 3.883 | 300 | 58.7 | −8.793 |
| | 350 | 58.9 | −8.780 |
| | 400 | 59.3 | −8.767 |
| | 450 | 59.4 | −8.754 |
| 4.057 | 100 | 87.6 | −8.744 |
| | 125 | 87.8 | −8.738 |
| | 300 | 88.5 | −8.692 |
| | 400 | 88.9 | −8.666 |
| | 500 | 89.2 | −8.640 |
| 4.242 | 400 | 123.6 | −8.525 |
| | 500 | 124.1 | −8.499 |
| | 600 | 124.5 | −8.474 |
| | 700 | 124.8 | −8.447 |
| 4.437 | 600 | 165.0 | −8.290 |
| | 700 | 165.2 | −8.263 |
| | 800 | 165.7 | −8.237 |
| | 900 | 165.8 | −8.211 |
| 4.645 | 1100 | 213.6 | −7.925 |
| | 1300 | 214.4 | −7.872 |
| | 1500 | 215.3 | −7.820 |
| | 1700 | 216.4 | −7.767 |
| 4.867 | 1000 | 268.1 | −7.661 |
| | 1400 | 269.2 | −7.557 |
| | 1600 | 270.2 | −7.506 |
| | 1800 | 270.6 | −7.450 |
| 5.102 | 2200 | 333.6 | −6.998 |
| | 2500 | 334.9 | −6.920 |
| | 3300 | 339.5 | −6.715 |
| | 3500 | 339.2 | −6.659 |
| 5.353 | 2600 | 409.7 | −6.478 |
| | 2800 | 410.4 | −6.424 |
| | 3000 | 408.6 | −6.370 |
| | 3200 | 411.3 | −6.316 |
| 5.620 | 3500 | 495.6 | −5.749 |
| | 4000 | 498.5 | −5.617 |
| | 4500 | 497.8 | −5.484 |
| | 5000 | 502.2 | −5.349 |
| 5.906 | 5000 | 600.0 | −4.777 |
| | | [600.7] | [−4.788] |
| | 5500 | 601.4 | −4.647 |
| | | [602.0] | [−4.650] |
| | 6000 | 603.4 | −4.509 |
| | | [602.6] | [−4.504] |
| | 6500 | 604.0 | −4.371 |
| | | [606.2] | [−4.355] |
| 6.212 | 7750 | 720.6 | −3.358 |
| | | [721.4] | [−3.292] |
| | 8000 | 719.5 | −3.287 |
| | | [722.1] | [−3.208] |
| | 8250 | 720.4 | −3.214 |
| | | [724.2] | [−3.125] |
| | 8500 | 721.5 | −3.131 |
| | | [725.6] | [−3.029] |

TABLE II. Equation of state data used in interpolating the Hugoniot data presented in Table IV. Quantities enclosed in square brackets were obtained with $T_e=T$ while unbracketed quantities were obtained with $T_e=0$ K. The reference state is $\rho_0=3.473$ g/cm$^3$, $T=300$ K, $P_0\approx 0$ GPa, and $E_0=-8.89$ eV/atom

| $\rho$ (g/cm$^3$) | $T$ (K) | $P$ (GPa) | $E$ (eV/at.) |
|---|---|---|---|
| 6.889 | 6500 | 951.3 | −0.808 |
| | | [953.9] | [−0.607] |
| | 7000 | 949.5 | −0.465 |
| | | [951.0] | [−0.355] |
| | 7750 | 950.4 | −0.161 |
| | | [951.7] | [0.007] |
| | 8000 | 950.4 | −0.052 |
| | | [953.6] | [0.091] |
| 7.073 | 7500 | 1023.1 | 0.199 |
| | | [1025.0] | [0.373] |
| | 8000 | 1023.4 | 0.392 |
| | | [1025.9] | [0.545] |
| | 8500 | 1025.7 | 0.510 |
| | | [1029.2] | [0.734] |
| | 9000 | 1028.1 | 0.715 |
| | | [1032.8] | [0.907] |
| 7.264 | 8500 | [1107.4] | [1.209] |
| | 9000 | 1107.8 | 1.185 |
| | | [1111.2] | [1.372] |
| | 9500 | 1110.3 | 1.333 |
| | | [1114.2] | [1.524] |
| | 10,000 | 1112.5 | 1.462 |
| | | [1118.2] | [1.680] |
| | 10,500 | 1115.9 | 1.588 |
| 7.462 | 11,000 | [1210.2] | [2.453] |
| | 11,500 | [1214.6] | [2.586] |
| | 12,000 | 1209.2 | 2.464 |
| | | [1217.5] | [2.728] |
| | 12,500 | 1210.5 | 2.557 |
| | | [1221.4] | [2.858] |
| | 13,000 | 1217.0 | 2.680 |
| | 13,500 | 1218.8 | 2.799 |
| 7.668 | 15,000 | [1334.0] | [4.034] |
| | 15,500 | [1339.5] | [4.157] |
| | 16,000 | [1344.4] | [4.288] |
| | 16,500 | 1330.3 | 3.941 |
| | | [1346.3] | [4.414] |
| | 17,000 | 1335.2 | 4.047 |
| | 17,500 | 1336.7 | 4.150 |
| | 18,000 | 1339.5 | 4.244 |

TABLE III. Hugoniot data for solid phase. Uncertainties in the last digit of the interpolation are given in parentheses. Quantities enclosed in square brackets were obtained with $T_e=T$ while unbracketed quantities were obtained with $T_e=0$ K. $\Delta E$ is the energy gap (defined when $T_e=0$) for our 64–atom supercell.

| $\rho$ (g/cm$^3$) | $T$ (K) | $P$ (GPa) | $\Delta E$ (eV) |
|---|---|---|---|
| 3.564 | 300(1) | 11.8(0) | 4.05(1) |
| 3.719 | 312(1) | 33.4(0) | 4.21(1) |
| 3.883 | 341(0) | 58.9(0) | 4.31(1) |
| 4.057 | 405(0) | 88.9(0) | 4.32(1) |
| 4.242 | 533(1) | 124.2(0) | 4.39(1) |
| 4.437 | 751(1) | 165.4(1) | 4.39(2) |
| 4.645 | 1083(3) | 213.4(1) | 4.39(5) |
| 4.867 | 1580(5) | 270.0(1) | 4.23(1) |
| 5.102 | 2250(19) | 333.9(5) | 4.14(3) |
| 5.353 | 3213(28) | 410.4(11) | 3.81(4) |
| 5.620 | 4531(22) | 499.6(8) | 3.46(2) |
| 5.906 | 6253(14) | 603.6(3) | 2.97(2) |
| | [6229(13)] | [604.5(7)] | [3.01(3)] |
| 6.212 | 8276(9) | 720.7(5) | 2.31(2) |
| | [8064(9)] | [723.0(2)] | [2.27(1)] |

TABLE IV. Hugoniot data for liquid phase. Uncertainties in the last digit of the extrapolation are given in parentheses. Quantities enclosed in square brackets were obtained with $T_e=T$ while unbracketed quantities were obtained with $T_e=0$ K. $Q$ is the average coordination number.

| $\rho$ (g/cm$^3$) | $T$ (K) | $P$ (GPa) | $Q$ |
|---|---|---|---|
| 6.889 | 7147(62) | 950.4(4) | 4.50(2) |
| | [6852(44)] | [952.7(11)] | [4.45(1)] |
| 7.073 | 8243(47) | 1025.0(4) | 4.75(1) |
| | [7735(19)] | [1025.5(7)] | [4.81(2)] |
| 7.264 | 10,238(32) | 1114.2(3) | 5.14(2) |
| | [9503(7)] | [1114.5(2)] | [5.17(1)] |
| 7.462 | 13,417(57) | 1218.6(12) | 5.66(44) |
| | [12,216(23)] | [1219.3(3)] | [5.76(5)] |
| 7.668 | 17,917(48) | 1339.3(9) | 6.15(6) |
| | [15,890(41)] | [1342.2(8)] | [6.36(5)] |

[1] L. R. Benedetti, J. H. Nguyen, W. A. Caldwell, H. Liu, M. Kruger, and R. Jeanloz, Science **286**, 100 (1999).
[2] H. Hirai and K. Kondo, Science **253**, 772 (1991).
[3] P. Gustafson, Carbon **24**, 169 (1986).
[4] F. Occelli, P. Loubeyre, and R. Letoullec, Nat. Mater. **2**, 151 (2003).
[5] J. W. Shaner, J. M. Brown, C. A. Swenson, and R. G. McQueen, J. Phys. (Paris), Colloq. **45**, 235 (1984).
[6] M. N. Pavloskii, Sov. Phys. Solid State **13**, 741 (1971).
[7] D. K. Bradley, J. H. Eggert, D. G. Hicks, P. M. Celliers, S. J. Moon, R. C. Cauble, and G. W. Collins, Phys. Rev. Lett. **93**, 195506 (2004).
[8] H. Nagao, K. G. Nakamura, K. Kondo, N. Ozaki, K. Takamatsu, T. Ono, T. Shiota, D. Ichinose, K. A. Tanaka, K. Wakabayashi, K. Okada, M. Yoshida, M. Nakai, K. Nagai, K. Shigemori, and K. Otani, Phys. Plasmas **13**, 052705 (2006).
[9] P. Hohenberg and W. Kohn, Phys. Rev. **136**, B864 (1964).
[10] M. P. Desjarlais, J. D. Kress, and L. A. Collins, Phys. Rev. E **66**, 025401(R) (2002).
[11] B. Militzer, Phys. Rev. Lett. **97**, 175501 (2006).
[12] S. A. Bonev, B. Militzer, and G. Galli, Phys. Rev. B **69**, 014101 (2004).
[13] M. P. Desjarlais, Phys. Rev. B **68**, 064204 (2003).
[14] G. Galli, R. M. Martin, R. Car, and M. Parrinello, Phys. Rev. Lett. **63**, 988 (1989); Phys. Rev. B **42**, 7470 (1990).
[15] G. Galli, R. M. Martin, R. Car, and M. Parrinello, Phys. Rev. B **42**, 7470 (1990).
[16] G. Galli, R. M. Martin, R. Car, and M. Parrinello, Science **250**, 1547 (1990).
[17] M. P. Grumbach and R. M. Martin, Phys. Rev. B **54**, 15730 (1996).
[18] X. Wang, S. Scandolo, and R. Car, Phys. Rev. Lett. **95**, 185701 (2005).
[19] A. A. Correa, S. A. Bonev, and G. Galli, Proc. Natl. Acad. Sci. U.S.A. **103**, 1204 (2006).
[20] L. E. Fried and W. M. Howard, Phys. Rev. B **61**, 8734 (2000).
[21] W. Kohn and L. Sham, Phys. Rev. **140**, A1133 (1965).
[22] G. Kresse and J. Hafner, Phys. Rev. B **47**, 558 (1993); **49**, 14251 (1994); G. Kresse and J. Furthmüller, Comput. Mater. Sci. **6**, 15 (1996); Phys. Rev. B **54**, 11169 (1996).
[23] S. Nosé, Mol. Phys. **52**, 255 (1984); J. Chem. Phys. **81**, 511 (1984); W. G. Hoover, Phys. Rev. A **31**, 1695 (1985).
[24] G. Kresse and D. Joubert, Phys. Rev. B **59**, 1758 (1999).
[25] J. P. Perdew, K. Burke, and M. Ernzerhof, Phys. Rev. Lett. **77**, 3865 (1996).
[26] M. Städele, J. A. Majewski, P. Vogl, and A. Görling, Phys. Rev. Lett. **79**, 2089 (1997); M. Städele, M. Moukara, J. A. Majewski, P. Vogl, and A. Görling, Phys. Rev. B **59**, 10031 (1999).
[27] K. Kunc, I. Loa, and K. Syassen, Phys. Rev. B **68**, 094107 (2003).
[28] M. C. Payne, M. P. Teter, D. C. Allan, T. A. Arias, and J. D. Joannopoulos, Rev. Mod. Phys. **64**, 1045 (1992).
[29] Kresse (unpublished).
[30] D. Prendergast, J. C. Grossman, and G. Galli, J. Chem. Phys. **123**, 014501 (2005).
[31] T. R. Mattsson and M. P. Desjarlais, Phys. Rev. Lett. **97**, 017801 (2006).
[32] Y. B. Zeldovich and Y. P. Raizer, *Physics of Shock Waves and High-Temperature Hydrodynamic Phenomena* (Academic, New York, 1966).
[33] J. J. Erpenbeck, Phys. Rev. A **46**, 6406 (1992).
[34] K. Kondo and T. J. Ahrens, Geophys. Res. Lett. **10**, 281 (1983).
[35] The Hugoniot points in the solid phase were equilibrated from crystalline diamond, while the Hugoniot points in the liquid phase were equilibrated from a premelted diamond.
[36] The values were interpolated using a linear least squares fit. Weighted least squares fit and interpolations using higher polynomials did not make significant differences.
[37] D. Alfè and G. D. Price, J. Chem. Phys. **116**, 6170 (2002).
[38] S. Scandolo, G. L. Chiarotti, and E. Tosatti, Phys. Rev. B **53**, 5051 (1996).
[39] V. V. Kechin, Phys. Rev. B **65**, 052102 (2001).
[40] This corresponds to Shot Nos. 26332, 28693, 28695, and 28697 as listed in Table I of Ref. 8.
[41] In the notation used here, the first Brillouin zone point is the top of the valence band while the latter one is the bottom of the conduction band.
[42] S. Fahy, K. J. Chang, S. G. Louie, and M. L. Cohen, Phys. Rev. B **35**, 5856 (1987).
[43] M. P. Surh, S. G. Louie, and M. L. Cohen, Phys. Rev. B **45**, 8239 (1992).